# Effects of Disk Loading on Handling Qualities of Large-Scale, Variable-RPM Quadcopters

**Ariel Walter** waltea@rpi.edu PhD Student
**Robert Niemiec** niemir2@rpi.edu Research Scientist
**Farhan Gandhi** fgandhi@rpi.edu Redfern Professor, Director

Center for Mobility with Vertical Lift (MOVE)
Rensselaer Polytechnic Institute
Troy, NY United States

## ABSTRACT

The performance of Urban Air Mobility (UAM) scale quadcopters with fixed-pitch, variable-speed rotors is examined at different values of disk loading. Three 544kg (1200lb) aircraft are considered in hover with disk loadings of 287N/m$^2$, 574N/m$^2$, and 861N/m$^2$ (6psf, 12psf, and 18psf), corresponding to rotor radii of 1.2m, 0.86m, and 0.70m (4.0ft, 2.8ft, and 2.3ft). Optimized explicit-model-following controllers are designed to meet standard handling qualities criteria using CONDUIT. In trim, it is seen that increased disk loading results in increased power, but with reduced motor torque due to higher rotor speeds. Time domain simulations are considered in order to examine the peak torque required by the aircraft, which is used to estimate required motor weight. Based on a step command in heave rate, a 54% reduction (total reduction of 40.6kg) in motor weight is seen for the 18psf quadcopter. Assuming a step change in rotor speed, the peak torque required for the heave maneuver is also predicted in closed form using an analytical model based on momentum and blade element theory. The analytical model captures the trend in peak torque during the heave rate step response, with predicted values within 12% of the values from the time domain simulation.

## NOTATION

**Symbols**

| | |
|---|---|
| $c_{l\alpha}$ | Lift Slope |
| $c_T$ | Rotor Thrust Coefficient |
| $c_Q$ | Rotor Torque Coefficient |
| $i$ | Motor Current |
| $I_r$ | Rotor Inertia |
| $K_t$ | Motor Torque Constant |
| $N_{rotors}$ | Number of Rotors |
| r | Yaw Rate |
| $R$ | Rotor Radius |
| t | Time |
| T | Thrust |
| $Q$ | Motor Torque |
| u | Longitudinal Velocity |
| U | Control Inputs |
| v | Lateral Velocity |
| $v$ | Induced Velocity |
| $V$ | Motor Voltage |
| $V_c$ | Climb Rate |
| w | Heave Rate |
| $M_{motor}$ | Motor Mass |
| X | Dynamic States |
| $\alpha_0$ | Zero Lift Angle of Attack |
| $\theta$ | Pitch Attitude |
| $\theta_0$ | Blade Root Pitch |
| $\theta_{tw}$ | Blade Twist |
| $\lambda$ | Inflow Ratio |
| $\rho$ | Air Density |
| $\sigma$ | Rotor Solidity |
| $\tau$ | Time Constant |
| $\phi$ | Roll Attitude |
| $\psi$ | Heading |
| $\Psi$ | Azimuthal Location |
| $\Omega$ | Rotor Speed |
| $\dot{\Omega}$ | Rotor Acceleration |

**Acronyms**

| | |
|---|---|
| ACAH | Attitude Command, Attitude Hold |
| eVTOL | Electric Vertical Takeoff and Landing |
| HQ | Handling Qualities |
| OLOP | Open-Loop-Onset-Point |
| RCDH | Rate Command, Direction Hold |
| RMAC | Rensselaer Multicopter Analysis Code |
| RMS | Root Mean Square |

## INTRODUCTION

The feasibility of the use of multirotor aircraft with variable-RPM rotors for Urban Air Mobility (UAM) applications is being examined. A large variety of electric Vertical Take-off and Landing (eVTOL) multicopter configurations have been proposed, but the field still faces many challenges before large eVTOL aircraft become commonplace (Ref. 1).

Presented at the Vertical Flight Society's 77th Annual Forum & Technology Display, Palm Beach, Florida, USA, May 11–13, 2021.

One such challenge is the ability of these large, electric aircraft to meet handling qualities requirements while using fixed-pitch, variable-RPM rotors. Though handling qualities requirements specific to these aircraft have not yet been officially established, existing military handling qualities can be applied, such as the requirements found in the ADS-33E-PRF (Ref. 2) and disturbance rejection criteria (Ref. 3). Further, a research group through the US Army (Ref. 4) incorporated gust rejection into the control design of a 3lb quadcopter and demonstrated its ability to hold position in turbulent conditions. The disturbance rejection capabilities of a reconfigurable multicopter with 4, 6, and 8 rotors were then examined (Ref. 5), where the quadcopter (highest disk loading) was able to hold its position the best in turbulent conditions.

It has previously been shown at Rensselaer Polytechnic Institute (Refs. 6–8) that manned-sized eVTOL aircraft which rely on changing the rotational speed of large rotors for control may struggle to meet handling qualities metrics without a significantly greater motor and drivetrain weight than current design trends indicate. Walter et al. (Ref. 6) previously examined the handling qualities of quadcopters of increasing sizes, finding that larger aircraft require a higher fraction of their gross weight to be dedicated to electric motors in order to provide sufficient torque for maneuverability. Ref. 7 examined the handling qualities of similar multicopters (same disk loading and gross weight of 544kg) with an increasing number of rotors, concluding that each aircraft required roughly the same motor weight fraction. Despite the increase in number of motors, the aircraft with more, smaller rotors were found to require relatively less torque to maneuver. The benefits of variable collective pitch rotors were examined in Ref. 8, where a 1252lb quadcopter was found to be limited by yaw maneuverability with both control types. This was alleviated through the use of rotor cant.

Malpica and Withrow-Maser at NASA (Refs. 9, 10) have also examined the handling qualities of UAM-scale multicopters. Malpica considered 1 to 6 passenger quadcopters with and without collective pitch control in Ref. 9 and found that the aircraft which relied on rotors with variable-RPM alone were unable to meet stability requirements with the assumed drivetrain. The effects of adding additional rotors to the 6 passenger multicopter was examined in Ref. 10, where it was found that the configurations with more rotors achieved faster rotor speed response, and therein better handling qualities performance.

These previous studies all utilize frequency-domain simulations in order to examine the handling qualities performance of the multicopters at an assumed disk loading. In Refs. 6, 7 a disk loading of 6psf was asssumed, while Ref. 8–10 used 2.5-3psf. Compared to commercial UAM concepts that are in development, these values may not be representative. For example, the Aurora Pegasus PAV has a disk loading of about 12psf (Ref. 11).

The present work aims to examine the effects of increased disk loading on the torque and power requirements needed to meet handling qualities specifications. Additionally, the results are compared to torque and power predicted by lower-order analytical models. Increasing the disk loading will increase induced power, but many eVTOL aircraft are designed to transition to wing-borne flight shortly after takeoff, which lessens the penalties in energy consumption (battery weight) compared to the penalties that would exist for more conventional VTOL designs. If gross weight is maintained, a higher disk loading will imply a smaller rotor, which will be easier to speed up/slow down due to its lower inertia (as observed in Ref. 12). In turn, this will reduce the required torque to execute thrust-dominated maneuvers (heave, roll, and pitch), potentially leading to reductions in motor weight (as weight is correlated with maximum motor torque, Ref. 13)

## MODELING AND ANALYSIS

### Platform

Cross-type quadcopters with gross weights of 544kg (1200lb) are considered in this study (nominally the same 1200lb aircraft in Ref. 6) with three different values of disk loading. The nominal configuration has a disk loading of 287N/m$^2$ (6psf) with a tip clearance of 10% of the rotor radius (Fig. 1a). The disk loading of the aircraft is increased by reducing the rotor size while keeping the gross weight and boom length constant, shown in Fig. 1b.

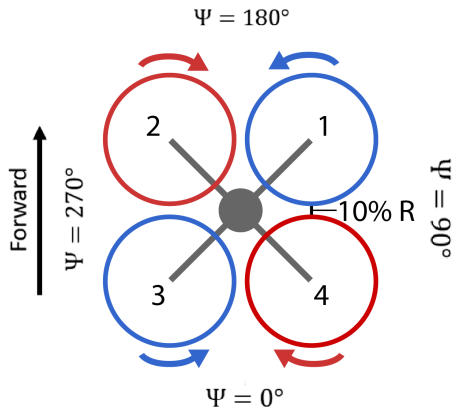


(a) Nominal Configuration with Rotor Numbering

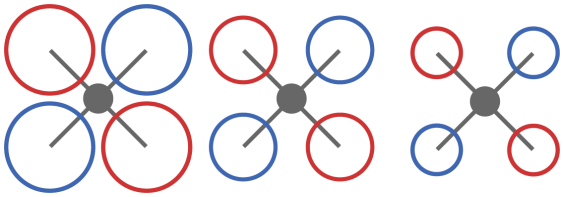

(b) Quadctoper with Increasing Disk Loading

Figure 1: Quadcopter Configurations

Listed in Table 1, many aircraft parameters remain the same regardless of the disk loading. The non-dimensional rotor parameters, like solidity, twist, and taper ratio, are held constant. The fuselage is also unchanged by the increased disk loading,

with rotational inertia based on a scaling of the NASA Concept quadcopter described in Ref. 1. Due to the symmetry of the platform, it is assumed that $I_{xy} = I_{xz} = I_{yz} = 0$.

Table 1: Aircraft Parameters

| Parameter | Value |
|---|---|
| Rotor Solidity | 0.09 |
| Taper Ratio | 2.5 |
| Root Pitch | 21.5° |
| Tip Pitch | 11.1° |
| Fuselage $I_{xx}$ | 467 kg m$^2$ |
| Fuselage $I_{yy}$ | 549 kg m$^2$ |
| Fuselage $I_{zz}$ | 905 kg m$^2$ |

The rotors are scaled as the disk loading is increased, with parameters listed in Table 2. Three cases are considered, ranging from 287N/m$^2$ (6psf) to 861N/m$^2$ (18psf). Rotor inertia scales with the fifth power of rotor radius (Ref. 12), so the smallest rotors have 15.6 times less rotational inertia than the largest (scales with $DL^{-5/2}$).

Table 2: Scaled Parameters

| Parameter | 6psf | 12psf | 18psf | Trend |
|---|---|---|---|---|
| DL (N/m$^2$) | 287 | 574 | 861 | $DL$ |
| Radius (m) | 1.2 | 0.86 | 0.70 | $DL^{-0.5}$ |
| Inertia (kg m$^2$) | 1.99 | 0.35 | 0.13 | $DL^{-5/2}$ |
| Motor $K_t$ (N m/A) | 1.17 | 0.70 | 0.51 | $DL^{-3/4}$ |

### Simulation Model

Linear dynamic simulation models are developed using the Rensselaer Multicopter Analysis Code (RMAC, Ref. 14). The rotors are modeled using blade element theory with a 10-state Peters-He dynamic wake model (Ref. 15). The inflow states are very high frequency (Ref. 16) relative to the rigid body dynamics and are reduced out of the model via static condensation. Motor dynamics are modeled within the simulation using DC motor equations (Eq. 1).

$$\begin{aligned} I\dot{\Omega} &= \underbrace{K_e i}_{\text{Motor Torque}} - \underbrace{Q_{\text{Aero}}}_{\text{External Torque}} \\ i &= \frac{1}{R_a}\left( \underbrace{V}_{\text{Input Voltage}} - \underbrace{K_e \Omega}_{\text{Back-EMF}} \right) \end{aligned} \tag{1}$$

Parameters of Eq. 1 (namely, $K_e$ and $R_a$) are derived as in Ref. 10. With this motor model, the motor voltages become the inputs to the system, with the rotor speeds included in the states. Along with the typical 12 rigid-body states, the reduced-order model for the quadcopter has 16 states (Eq. 2) with 4 inputs (Eq. 3).

$$X = \begin{bmatrix} x & y & z & \phi & \theta & \psi & u & v & w & p & q & r & \Omega_1 & \Omega_2 & \Omega_3 & \Omega_4 \end{bmatrix}^T \tag{2}$$

$$U = \begin{bmatrix} V_1 & V_2 & V_3 & V_4 \end{bmatrix}^T \tag{3}$$

Control mixing is defined using multi-rotor coordinates (Ref. 17) such that the dynamics of the aircraft become decoupled and can be treated as a system of single-input, single-output systems. Shown in Eq. 4, the rotor azimuthal location ($\Psi_k$) is used to transform the inputs, with collective ($V_0$), roll ($V_{1s}$), pitch ($V_{1c}$), and differential ($V_d$) inputs for the vertical, lateral, longitudinal, and directional axes of the aircraft, respectively.

$$\begin{bmatrix} V_1 \\ V_2 \\ V_3 \\ V_4 \end{bmatrix} = \begin{bmatrix} 1 & \sin(\Psi_1) & \cos(\Psi_1) & 1 \\ 1 & \sin(\Psi_2) & \cos(\Psi_2) & -1 \\ 1 & \sin(\Psi_3) & \cos(\Psi_3) & 1 \\ 1 & \sin(\Psi_4) & \cos(\Psi_4) & -1 \end{bmatrix} \begin{bmatrix} V_0 \\ V_{1s} \\ V_{1c} \\ V_d \end{bmatrix} \tag{4}$$

### Control Optimization

An ACAH/RCDH explicit-model-following control architecture (Fig. 2) is implemented in order to stabilize and control the aircraft in hover. Commanded rotor speeds are filtered through a first-order command model, which controls the rise time of the rotor speed response. The motor model is inverted in order to determine voltage inputs from the filtered rotor speeds. The differential command is fed through directly as

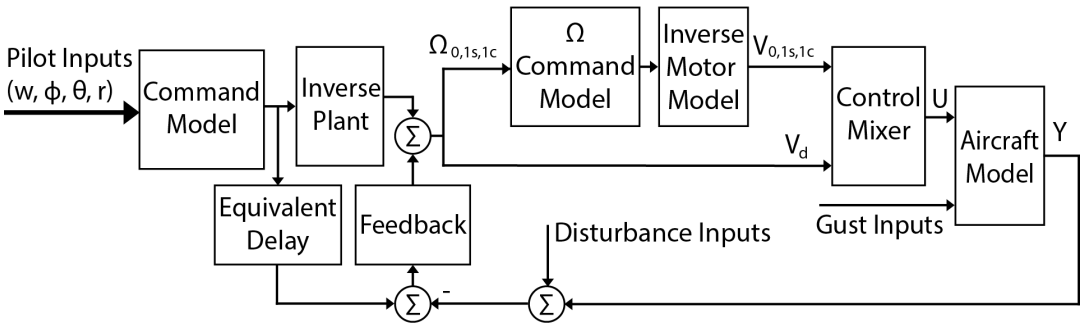


Figure 2: Controller Architecture

a voltage without filtering, since the yaw response relies on changes in torque rather than changes in thrust. The modeling of the motor dynamics causes an associated lag, which is approximated and included in the feedback path as an equivalent delay. This synchronization of the feedback path improves model following at high frequency.

The command model parameters and feedback gains are optimized using CONDUIT® (Ref. 18) to minimize actuator effort while meeting standard Level 1 handling qualities criteria. Listed in Table 3, CONDUIT® handling qualities specifications from the ADS-33E-PRF (Ref. 2), disturbance rejection requirements (Ref. 3), and Open-Loop Onset Point (OLOP, Ref. 19) specifications are included.

Table 3: CONDUIT® Constraints

| Specification | Axes |
|---|---|
| *Hard Constraints* | |
| Eigenvalues | All |
| Stability Margins | All |
| Nichols Margin | All |
| *Soft Constraints* | |
| Bandwidth/Phase Delay | Roll, Pitch, Yaw |
| Crossover Frequency | All |
| Disturbance Rejection Bandwidth | All |
| Disturbance Rejection Peak | All |
| Damping | All |
| Heave Mode | Heave |
| Model Following | All |
| OLOP (Pilot) | All |
| OLOP (Disturbance) | All |
| *Summed Objectives* | |
| Actuator RMS (Pilot) | All |
| Actuator RMS (Disturbance) | All |
| Crossover Frequency | All |

Table 4: Hover Trim Parameters

| | 6 psf | 12 psf | 18 psf | Trend |
|---|---|---|---|---|
| Ω (RPM) | 1380 | 2140 | 3150 | $DL$ |
| Tip Speed (Mach) | 0.40 | 0.56 | 0.68 | $\sqrt{DL}$ |
| Power (kW) | 21.1 | 29.5 | 35.7 | $\sqrt{DL}$ |
| Torque (N m) | 176 | 125 | 102 | $DL^{-0.5}$ |
| Current (A) | 150 | 179 | 199 | $DL^{0.25}$ |

Table 5: Heave Design Parameters

| Design Parameter | 6psf | 12psf | 18psf |
|---|---|---|---|
| Ω Time Constant | 0.090 | 0.091 | 0.091 |
| Heave Time Constant | 4.7 | 4.7 | 4.7 |
| Proportional Gain | 5.9 | 11.8 | 17.0 |
| Integral Ratio | 0.2 | 0.2 | 0.2 |

# RESULTS

## Trim Results

As the rotors become smaller, the rotational speed needed to maintain the same level of thrusts increases. In fact, the rotor speed increases linearly with the disk loading (this trend implies that $C_T$ does not change with the rotor radius/disk loading). As the rotor radius is inversely proportional to $\sqrt{DL}$ (thrust is held constant), it follows that the tip speed is proportional to $\sqrt{DL}$. It is also observed that the power consumption scales with the square root of disk loading, which together with the trend in rotor speed implies that torque is inversely proportional to $\sqrt{DL}$.

By the design process of Ref. 9, the nominal operating voltage and current are assumed to be the same, such that Current $\propto \sqrt{\text{Power}}$, which implies that current should be proportional to $DL^{0.25}$, which is borne out by the analysis. These trends, and the values obtained via RMAC simulation are listed in Table 4. For the aircraft considered, the tip speed nears Mach 0.7 for the 18psf case, suggesting that further increase of the disk loading may not be feasible without encountering transonic flow.

## Heave Controller

Design parameters for the optimization of the heave controller are listed in Table 5 with the handling qualities metrics listed in Table. 6. The heave command model time constant is held constant such that all cases will follow the same heave commands and have an appropriately located heave mode pole. An integral ratio of 1/5 of the minimum crossover frequency (1 rad/s) is also held constant (Ref. 18). The optimization settles to roughly the same rotor speed command model time constant for all cases, while the heave proportional gain tends to vary linearly with the disk loading. Shown in Table 6, with the optimization complete, the disturbance rejection bandwidth and heave mode pole fall on the Level 1/2 boundary.

Table 6: Heave Handling Qualities

| HQ Parameter | 6psf | 12psf | 18psf |
|---|---|---|---|
| Gain Margin (dB) | 51 | 50 | 49 |
| Phase Margin (deg) | 87 | 84 | 81 |
| Crossover Frequency (rad/s) | 1.04 | 1.10 | 1.14 |
| Disturbance Rejection Bandwidth (rad/s) | 1.0* | 1.0* | 1.0* |
| Disturbance Rejection Peak (dB) | 0.58 | 0.63 | 0.65 |
| Heave Response Time Constant (s) | 5* | 5* | 5* |
| Heave Delay (s) | 0.08 | 0.08 | 0.08 |
| Command Model Following | 14.6 | 14.8 | 14.9 |
| OLOP Phase - Pilot (dB) | - | - | - |
| OLOP Magnitude - Pilot (deg) | - | - | - |
| OLOP Phase - Disturbance (dB) | -108 | -126 | -98 |
| OLOP Magnitude - Disturbance (deg) | -11 | -18 | -1.1 |
| Actuator RMS - Pilot | 0.10 | 0.26 | 0.45 |
| Actuator RMS - Disturbance | 0.30 | 0.82 | 1.44 |

* Limiting - No open loop onset point in frequency range

**Heave Time Domain Simulations**

The primary time-domain simulation considered is a climb rate step response. As was concluded in Ref. 6, required motor torque was greatest during a heave step for a 544 kg aircraft with an ACAH controller. Though this may change with increased disk loading as the yaw response becomes limiting, it has been suggested that yaw authority is best increased by the addition of rotor cant for multirotor aircraft (Ref. 8). Thus, a step in heave rate is simulated in order to examine aircraft performance in the time domain.

A climb rate of 5 m/s is commanded (a negative value since positive is defined downward), and all cases follow the command exactly (Fig. 3). Because heave is governed by collective input only (Eq. 4), all four rotors on any vehicle will behave identically in terms of speed, torque required, and power consumption. The rotor speeds during the heave step for each disk loading case are shown in Fig. 4, along with the hover rotor speeds. At higher disk loading (smaller rotor radius), both higher trim rotor speed and change in rotor speed are required.

Similarly, shown in Fig. 5, with higher disk loading an increase in both the trim power (from 26 to 40 kW for a disk loading of 6psf and 18psf) and peak power (from 38 to 44 kW) occurs. However, the difference between the trim and peak power decreases (from 12 to 3.9 kW) as disk loading grows, suggesting that the power delivery capability for the drivetrain may not be as significantly different for different disk loadings. Fig. 6 shows the torque required by each configuration, with the smaller rotors (corresponding to higher disk loading) requiring the least torque, both in steady state operation, and during the transient (125 Nm, as opposed to 307 Nm required for the 6 psf rotor). The peak speed, power, and torque (and their increment over the hover value) for each configuration is summarized in Table 7.

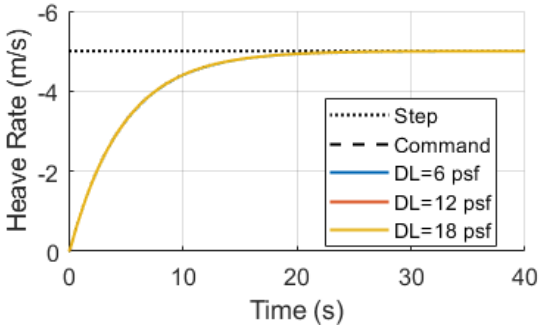


Figure 3: Heave Step Response

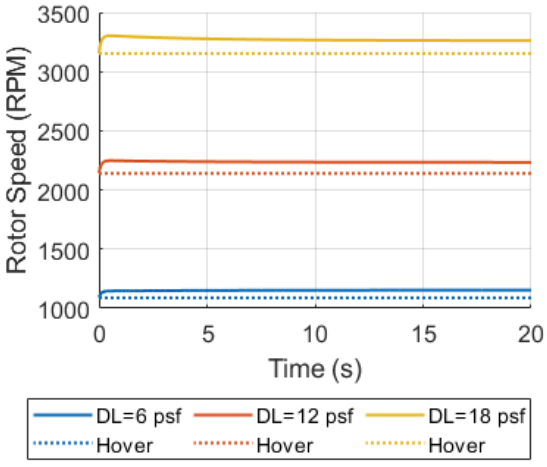


Figure 4: Rotor Speed During Heave Step

Table 7: Motor/Rotor Requirements for Heave Step

| | 6psf | 12psf | 18psf |
|---|---|---|---|
| $\Delta\Omega$ (RPM) | 65.4 | 93.3 | 108 |
| Peak Power (kW) | 38.2 | 40.8 | 44.4 |
| $\Delta$Power (kW) | 3.8 | 5.0 | 5.9 |
| Peak Torque (N m) | 307 | 169 | 125 |
| $\Delta$ Torque (N m) | 20.7 | 13.7 | 11.0 |

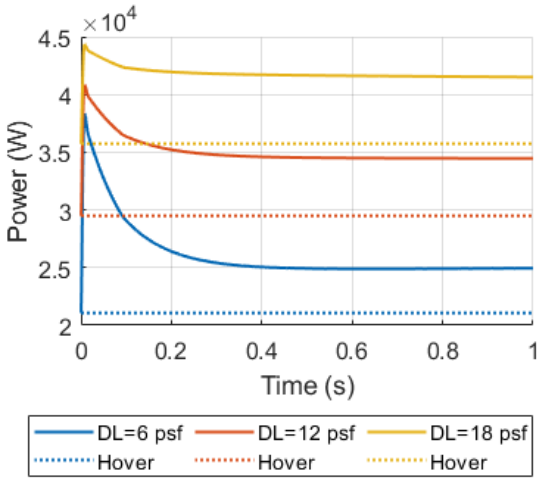


Figure 5: Motor Power During Heave Step

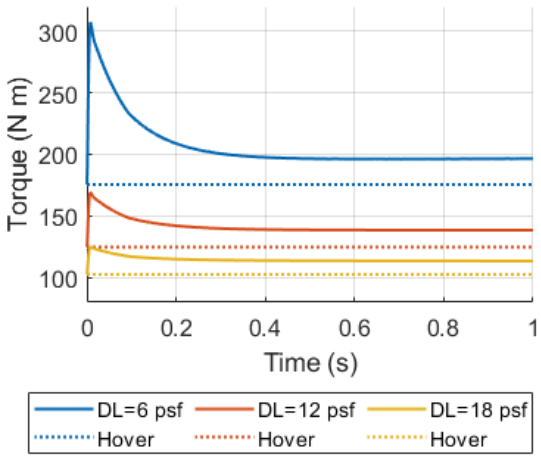


Figure 6: Motor Torque During Heave Step

### Low-Order Analytical Modeling

Though the RMAC-based analysis is effective for the prediction of the flight dynamics of multicopters, it requires a fully-tuned controller to make any estimations of torque requirements during maneuvers. For initial sizing, full dynamic simulations may not be available to tune controllers. Even if they are, changes to the vehicle could substantially alter the dynamics, requiring re-optimization of the controller with each update.

To streamline the sizing process, an analytical model is presented. Consider torque balance on the rotor during acceleration. The torque needed from the motor is a combination of the torque needed to overcome aerodynamic drag, $Q_{\text{aero}}$, and the torque needed to accelerate the rotor $I\dot{\Omega}$.

$$Q_{\text{motor}} = Q_{\text{aero}} + I\dot{\Omega} \tag{5}$$

Consider the case where $\Omega$ is required to follow a first-order command. In this case, if a step command of magnitude $\Delta\Omega$ is issued, the actual rotor speed will be

$$\begin{aligned} \delta\Omega &= \Omega(t) - \Omega_{\text{hover}} = \Delta\Omega(1 - e^{-t/\tau}) \\ \dot{\Omega} &= \frac{\Delta\Omega}{\tau} e^{-t/\tau} \end{aligned} \tag{6}$$

where $\tau$ is the time constant defining the first-order command model. By observation of Fig. 6, it is clear that the peak torque occurs at the beginning of the heave command. Substituting Eq. 6 into Eq. 5 and evaluating at $t = 0$ yields

$$Q_{\text{peak}} = Q_{\text{hover}} + \frac{I}{\tau}\Delta\Omega \tag{7}$$

$Q_{\text{hover}}$ can be expressed in terms of $C_T$, $C_Q$, $R$, and $T$.

$$Q_{\text{hover}} = \frac{C_Q R}{C_T} T \tag{8}$$

Using blade element theory with the assumption of uniform inflow, the thrust and torque coefficients are approximated by Eq. 9, (Ref. 20), where $\alpha_0$ is the zero-lift angle of attack for the airfoil used in the rotor. Equation 9 is dependent only on the nondimensional parameters of the rotor (e.g. solidity, twist), which are identical for all rotors considered in this study (Reynolds number effects are neglected). Thus, if the thrust is held constant the hover torque should scale linearly with the radius of the rotor (or with $DL^{-0.5}$), which is borne out by the RMAC analysis (Table 4).

$$\begin{aligned} C_T &= \frac{\sigma C_{L_\alpha}}{2}\left[\frac{\theta_{75} - \alpha_0}{3} - \frac{\lambda}{2}\right] \\ C_Q &= \frac{C_T^{3/2}}{\sqrt{2}} + \frac{\sigma C_{d0}}{8} \end{aligned} \tag{9}$$

To estimate the torque required for acceleration, two parameters need to be determined. Specifically, the time constant, $\tau$, and the change in rotor speed $\Delta\Omega$. For $\Delta\Omega$, blade element theory can once again be used, with inflow modified for climb. From Leishman (Ref. 20), the induced velocity through the rotor plane is given in terms of climb rate $V_c$ and hover induced velocity $v_h = \sqrt{T/2\rho A}$

$$\frac{v_i}{v_h} = \frac{V_c}{2v_h} + \sqrt{\left(\frac{V_c}{2v_h}\right)^2 + 1} \tag{10}$$

which implies that the total velocity through the rotor is

$$v_i + V_c = \frac{V_c}{2} + \sqrt{\left(\frac{V_c}{2}\right)^2 + \frac{T}{2\rho A}} \tag{11}$$

From Eq. 9 and the definition of thrust coefficient,

$$T = \rho A V_{\text{tip}}^2 \frac{\sigma C_{L_\alpha}}{2}\left[\frac{\theta_{75} - \alpha_0}{3} - \frac{\lambda}{2}\right] \tag{12}$$

Distributing $V_{\text{tip}}^2$ yields

$$T = \rho A \frac{\sigma C_{L_\alpha}}{2}\left[\frac{\theta_{75} - \alpha_0}{3} V_{\text{tip}} - \frac{V_{\text{tip}} V}{2}\right] \tag{13}$$

where $V = v_i + V_c = \lambda V_{\text{tip}}$. Solving the quadratic for $V_{\text{tip}}$,

$$V_{\text{tip}} = \frac{\frac{3V}{2} + \sqrt{\left(\frac{3V}{2}\right)^2 + \frac{24T(\theta_{75} - \alpha_0)}{\rho\sigma A C_{L_\alpha}}}}{2(\theta_{75} - \alpha_0)} \tag{14}$$

and $\Delta\Omega = V_{tip}/R - \Omega_{\text{hover}}$.

The time constant $\tau$ will influence stability (mainly phase margin) and handling qualities (bandwidth, DRB, etc.), and can be determined from these requirements, and then used to estimate $Q_{\text{peak}}$ for motor sizing. Alternately, if the maximum torque is known (because a motor/drivetrain is selected), the lower bound on $\tau$ can be calculated by rearranging Eq. 7. This value of $\tau$ corresponds to the fastest possible acceleration, within the bounds of a first-order command and the drivetrain limits.

$$\tau = \frac{(Q_{\text{peak}} - Q_{\text{hover}})}{I\Delta\Omega} \tag{15}$$

For the time constants given in Table 6, the speed of the rotors (as determined via linear simulation) and the predictions based on Eq. 14 are plotted in Fig. 7. The analytical model does not capture the transient nor the steady-state value very well, though these differences are explainable. The transient is different for two reasons. First, the analytical model does not account for the transient thrust needed to actually accelerate the aircraft upward (this is more pronounced as the disk loading increases). Second, the slow decay toward steady-state values is associated with the heave command model, which is similarly absent from the analytical model.

On the other hand, the disagreement in steady-state value is believed to be a shortcoming of the *simulation* rather than the analytical model, as the closed-loop simulations use the linearized aircraft model, which does not capture the nonlinear

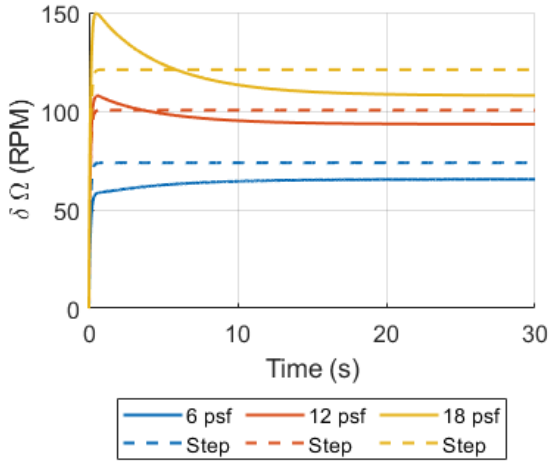


Figure 7: Rotor Speed During Heave Step and First-Order Approximation

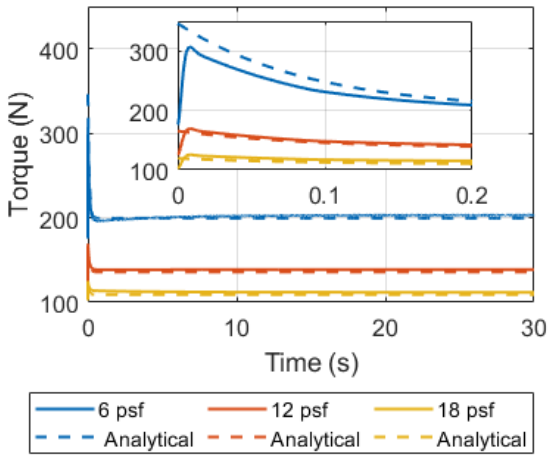


Figure 8: Motor Torque During Heave Step and Analytical Approximation

behavior of the induced flow in climb, while the analytical model does.

The torque predicted by the simulation and analytical models are plotted versus time in Fig. 8. Though the rotor speeds were different in both the transient and steady-state behavior, the torque required is remarkably similar both in trend and in magnitude, though the peak torque is overpredicted for the 6psf case. For the 12psf and 18psf cases, the peak torque is predicted within 2.5% and 5%, respectively. The change in rotor speed and peak torque for both the simulation and analytical model are listed in Table. 8.

Table 8: Torque Prediction Compared to Analytical Model

| | 6 psf | 12 psf | 18 psf |
|---|---|---|---|
| ΔΩ - Simulation (RPM) | 65.4 | 93.3 | 108 |
| ΔΩ - Analytical (RPM) | 73.8 | 101 | 121 |
| Peak Torque - Simulation (N m) | 307 | 169 | 125 |
| Peak Torque - Analytical (N m) | 346 | 165 | 119 |

### Motor Weight Approximations and Power Consumption

The necessary motor weight to provide the peak torque required to climb can be estimated by the peak torque in Fig. 8 using Eq. 16 (Ref. 13). Using the peak torques in Table 7, motor masses of 18.8kg, 11.2kg, and 8.7kg are estimated for the 6psf, 12psf, and 18psf configurations, respectively. Listed in Table 9, this is equivalent to a 54% total reduction in motor weight from the 6psf to 18psf cases, equal to 40.6kg on the 544kg aircraft. However, the hover power is increased by 70% over the nominal case, while the climb power is increased by 55%.

$$M_{motor} = 0.1372 Q_{peak}^{0.8587} \tag{16}$$

Table 9: Motor Weight and Power Consumption Comparison

| | 6 psf | 12 psf | 18 psf |
|---|---|---|---|
| Motor Mass (kg) | 18.8 | 11.2 (-40%) | 8.7 (-54%) |
| Hover Power (kW) | 21.1 | 29.5 (+40%) | 35.7 (+70%) |
| Climb Power (kW) | 25.9 | 34.3 (+32%) | 40.3 (+55%) |

## CONCLUSIONS

The effects of increasing disk loading were examined through simulation of three UAM-scale quadctopers (gross weight of 544kg) with decreasing rotor radii (corresponding to disk loadings of 6, 12, and 18psf). With optimized controllers designed to meet handling qualities specifications, a step in heave rate was simulated in the time domain in order to determine torque requirements during maneuvers.

Higher disk loading resulted in a reduction of peak torque requirement and motor weight predictions, with the predicted motor weight decreasing by 40.4kg from the 6psf to 18psf case. However, this reduction in torque came with a 70% increase in hover power consumption, consistent with momentum theory. However, the peak power requirements were not as disparate, with the 18psf quadcopter requiring only 16% greater peak power, suggesting that the power delivery requirements are not as sensitive to disk loading as aerodynamic analysis alone would imply.

"Back-of-the-envelope" estimations of the peak torque during a climb maneuver were developed using a torque balance and blade element theory with uniform inflow. By modeling the climb maneuver as a step change in rotor speed, very good estimations of the peak torque were obtained, without the need for a complete dynamics model and control optimization , predicting the peak torque within 12% (within 5% for the 12psf and 18psf cases) of the simulation values.

## ACKNOWLEDGMENTS

This work is carried out at Rensselaer Polytechnic Institute under the Army/Navy/NASA Vertical Lift Research Center of Excellence (VLRCOE) Program, grant number W911W61120012, with Dr. Mahendra Bhagwat as Technical Monitor. The authors would like to acknowledge the Army Combat Capabilities Development Command for sponsoring Ms. Walter through the Science Mathematics And Research Transformation Scholarship Program, as well as the Army Research Office for sponsoring Mr. McKay through the National Defense Science and Engineering Graduate Fellowship.

**Author Contact:**

Ariel Walter: waltea@rpi.edu
Michael McKay: mckaym2@rpi.edu
Robert Niemiec: niemir2@rpi.edu
Farhan Gandhi: fgandhi@rpi.edu

## REFERENCES

1. Johnson, W., Silva, C., and Solis, E., "Concept Vehicles for VTOL Air Taxi Operations," AHS Technical Conference on Aeromechanics Design for Transformative Flight, San Francisco, CA, January 16–18, 2018.

2. "Aeronautical Design Standard, Performance Specification, Handling Qualities Requirements for Military Rotorcraft," Technical Report ADS-33E-PRF, March 2000.

3. Berger, T., Ivler, C., Berrios, M., Tischler, M., and Miller, D., "Disturbance Rejection Handling-Qualities Criteria for Rotorcraft," 72nd Annual AHS Forum, West Palm Beach, FL, May 16–19, 2016.

4. Berrios, M., Berger, T., Tischler, M., Juhasz, O., and Sanders, F., "Hover Flight Control Design for UAS Using Performance-based Disturbance Rejection Requirements," AHS 73rd Annual Forum, Fort Worth, TX, May 9–11, 2017.

5. Lopez, M., Tischler, M., Juhasz, O., Gong, A., Sanders, F., Soong, J., and Nadell, S., "Flight Test Comparison of Gust Rejection Capability for Various Multicopter Configurations," VFS 75th Annual Forum & Technology Display, Philadelphia, PA, May 13–16, 2019.

6. Walter, A., McKay, M., Niemiec, R., Gandhi, F., and Ivler, C., "Hover Handling Qualities of Fixed-Pitch, Variable-RPM Quadcopters with Increasing Rotor Diameter," VFS International 76th Annual Forum, Virtual, October 6–8, 2020.

7. Bahr, M., McKay, M., Niemiec, R., and Gandhi, F., "Handling Qualities Assessment of Large Variable-RPM Multi-Rotor Aircraft for Urban Air Mobility," VFS International 76th Annual Forum, Virtual, October 6–8, 2020.

8. Niemiec, R., Gandhi, F., Lopez, M., and Tischler, M., "System Identification and Handling Qualities Predictions of an eVTOL Urban Air Mobility Aircraft Using Modern Flight Control Methods," 76th Annual VFS Forum, Virginia Beach, VA, October 6–8, 2020.

9. Malpica, C., and Withrow-Maser, S., "Handling Qualities Analysis of Blade Pitch and Rotor Speed Controlled eVTOL Quadrotor Concepts for Urban Air Mobility," VFS International Powered Lift Conference, San Jose, CA, January 21–23, 2020.

10. Withrow-Maser, S., Malpica, C., and Nagami, K., "Handling Qualities Analysis of Blade Pitch and Rotor Speed Controlled eVTOL Quadrotor Concepts for Urban Air Mobility," VFS International Powered Lift Conference, San Jose, CA, January 21–23, 2020.

11. Giannini, F., Kaufman, A., and Kearney, M., "Configuration Development and Subscale Flight Testing of an Urban Mobility eVTOL," AHS Technical Conference on Aeromechanics Design for Transformative Vertical Flight, San Francisco, CA, Jan 16–19, 2018.

12. Walter, A., McKay, M., Niemiec, R., Gandhi, F., Hamilton, C., and Jaran, C., "An Assessment of Heave Response Dynamics for Electrically Driven Rotors of Increasing Diameter," Autonomous VTOL Technical Meeting & eVTOL Symposium, Mesa,AZ, Janurary 2019.

13. Johnson, W., "NDARC – NASA Design and Analysis of Rotorcraft," NASA TP 218751, April 2015.

14. Niemiec, R., and Gandhi, F., "Development and Validation of the Rensselaer Multicopter Analysis Code (RMAC): A Physics-Based Comprehensive Modeling Tool," 75th Annual VFS Forum, Philadelphia, PA, May 13–16, 2019.

15. Peters, D., Boyd, D., and He, C. J., "Finite-State Induced-Flow Model for Rotors in Hover and Forward Flight," *Journal of the American Helicopter Society*, Vol. 34, (4), 1989, pp. 5–17.

16. Niemiec, R., *Development and Application of a Medium-Fidelity Analysis Code for Multicopter Aerodynamics and Flight Mechanics*, Ph.D. thesis, Rensselaer Polytechnic Institute, 2018.

17. Niemiec, R., and Gandhi, F., "Multi-rotor Coordinate Transform for Orthogonal Primary and Redundant Control Modes for Regular Hexacopters and Octocopters," 42nd European Rotorcraft Forum, Lille, France, September 5–8, 2016.

18. Tischler, M., Berger, T., Ivler, C., Mansur, M., Cheung, K., and Soong, J., *Practical Methods for Aircraft and Rotorcraft Flight Control Design: An Optimization-Based Approach*, AIAA Education Series, Reston, VA, 2017.

19. Duda, H., "Flight Control System Design Considering Rate Saturation," *Aerospace Science and Technology*, Vol. 4, 1998, pp. 265–275.

20. Leishman, J. G., *Principles of Helicopter Aerodynamics*, Cambridge University Press, New York, NY, 2000, Chapter 10.